

doi.org/10.1002/elan.202200398

Electroanalytical Study of Fungicide Bixafen on Paste Electrode Based on the Thermally Reduced Graphene Oxide Synthesized in Air Conditions and its Determination in River Water Samples

Mariola Brycht,^{*,[a]} Karolina Kowalewska,^[a] Sławomira Skrzypek,^[a] and Valentin Mirčeski^[a, b, c]

Abstract: An electrochemical study of the fungicide bixafen using a paste electrode based on thermally reduced graphene oxide (TRGOPE) synthesized in air is presented for the first time. Cyclic voltammetry and square-wave voltammetry (SWV) were conducted to characterize the mechanism of the underlying electrode process of bixafen. Optimization of the procedure for the

quantitative determination of bixafen was carried out by SWV. Excellent electroanalytical performance in terms of a limit of detection of 31.5 nmol L^{-1} was achieved. The TRGOPE was effectively employed to analyze bixafen in spiked river and tap water samples. The selectivity towards bixafen determination was also assessed.

Keywords: bixafen · paste electrode · pesticide · reduced graphene oxide · voltammetry

1 Introduction

Fungicides are substances used to kill or hamper the growth of parasitic fungi or fungal spores. Various classes of fungicides have been extensively used to control diseases in growing crops intended for the market to achieve high-quality products [1]. Fungicides are also used to control post-harvest diseases that might cause a breakdown of the commodity [2].

Nowadays, one of the most frequently used fungicides in agriculture are the new broad-spectrum fungicides from the succinate dehydrogenase inhibitor (SDHI) class [3,4] that are highly active against diseases affecting cereals, fruits, and vegetables [5]. SDHI fungicides inhibit the enzyme succinate dehydrogenase (SDH) in the mitochondrial respiratory chain (complex II) of target fungi [1,3,4,6]. The first generation of SDHI fungicides, such as carboxin and oxycarboxin, were introduced in the late 1960s; they did not however reach a widespread usage in agriculture due to their moderate effectiveness [5,7]. In the last decade, the next generation SDHI fungicides that exhibit a broad antifungal effect, such as boscalid, fluopyram, isopyrazam, penthiopyrad, fluxapyroxad, bixafen, and benzovindiflupyr, have been introduced into the market [1,5,7].

Bixafen, a pyrazole carboxamide fungicide, was introduced by Bayer CropScience and first launched in the market in 2011 in the United Kingdom [3,8]. It is a broad-spectrum systemic fungicide that is currently extensively used in agriculture to control fungal diseases in crops and boost production yields [3,4,6,9,10]. It is highly effective against *Septoria tritici*, *Puccinia triticina*, *Puccinia striiformis*, *Oculimacula spp.*, and *Pyrenophora tritici-repentis* in wheat [8]. Bixafen was found to have potential adverse

effects on the ecosystem as it is not easily biodegradable compound and shows high persistence and chemical stability in the environment, especially in soil [11]. Although bixafen is not significantly toxic to mammals, it is highly toxic to aquatic organisms [12]. Therefore, it is of the utmost importance to elaborate a novel, simple, and sensitive analytical procedure for the determination of this fungicide. Until now, a few analytical methods have been developed for bixafen determination and they are based on chromatography, *i. e.*, the liquid chromatography coupled with tandem mass spectrometry (LC-MS/MS) [9,13], ultra-high liquid chromatography coupled with tandem mass spectrometry (UHPLC-MS/MS) [5,14], gas chromatography coupled with mass spectrometry (GC-MS) [15], and gas chromatography coupled with tandem mass spectrometry (GC-MS/MS) [8,16]. The comparison of the validation parameters for the determination of bixafen by above-mentioned chromatographic techniques is presented in the Table 1. Although chromatographic methods show high accuracy, precision, sensitivity and

[a] M. Brycht, K. Kowalewska, S. Skrzypek, V. Mirčeski
University of Lodz, Faculty of Chemistry, Department of Inorganic and Analytical Chemistry, Tamka 12, 91-403 Lodz, Poland
E-mail: mariola.brycht@chemia.uni.lodz.pl

[b] V. Mirčeski
Ss. Cyril and Methodius University in Skopje, Faculty of Natural Sciences and Mathematics, Institute of Chemistry, Arhimedova 5, P.O. Box 162, 1001 Skopje, RN Macedonia

[c] V. Mirčeski
Macedonian Academy of Sciences and Arts, Research Center for Environment and Materials, Boulevard Krste Misirkov 2, 1000 Skopje, RN Macedonia

Table 1. The validation parameters for the determination of bixafen by chromatographic techniques.

Technique	LOD	LOQ	Reference
LC-MS/MS	482.8–2.2 nmolL ⁻¹	1.9–7.2 nmolL ⁻¹	[9]
LC-MS/MS	2.4–4.8 pmolL ⁻¹	12.1–24.1 pmolL ⁻¹	[13]
UHPLC-MS/MS	3.6 nmolL ⁻¹	N/A	[5]
UHPLC-MS/MS	724.3 pmolL ⁻¹	2.4–2.7 nmolL ⁻¹	[14]
GC-MS	17.6 nmolL ⁻¹	57.9 nmolL ⁻¹	[15]
GC-MS/MS	N/A	482.8 pmolL ⁻¹	[8]
GC-MS/MS	4.8 pmolL ⁻¹	120.7 nmolL ⁻¹	[16]

N/A – information not available.

exhibit low limits of detection and quantification, they require rather expensive and sophisticated equipment, well-trained staff, and labor-intensive and time-consuming sample pretreatment [17]. Therefore, currently, electrochemical techniques have become an attractive and promising alternative to chromatographic methods in the analysis of various compounds including pesticides. Electrochemical methods are characterized by a fast response, short analysis time, low cost, simplicity of use [18], and sample preparation is rather simple, requiring only dissolution of the sample in a solvent, and optionally, filtration and separation of the insoluble matrix components [19]. Other assets of electrochemical methods are the capability of miniaturization, and applicability for detection in real time [18]. According to our best knowledge, bixafen has not yet been investigated by electrochemical techniques.

Nowadays, enormous interest has been focused on the development of novel, environmentally friendly, and sensitive electrochemical sensors. Among all materials used to develop sensors, different types of carbon-based nanomaterials, *e.g.*, carbon nanotubes, carbon dots, graphene and its derivatives, have attracted the highest interest. In general, two types of sensors can be developed, depending on where carbon-based nanomaterial can be incorporated as an additive into electrodes or can be the main electrode material. Since the last decade, considerable interest has been paid to the incorporation of graphene and its derivatives into sensor technologies [20]. Graphene has an exceptional features, such as mechanical, optical, thermal, and electrical properties including high surface area and good conductivity [21]. Due to the hydrophobic nature of graphene, hydrophilic graphene derivatives, such as graphene oxide (GO) and reduced graphene oxide (RGO), have been more extensively used in the development of electrochemical sensors. RGO and GO have a similar structure to graphene [22,23], though, in contrary to graphene, they contain residual oxygen-containing groups and have some structural defects, predominantly in the basal plane [24,25]; however, their performance is satisfactory enough to be utilized for practical applications [23,26]. When comparing the properties of graphene with GO and RGO, the latter behaves as an intermediate state between graphene and GO [23]. To apply RGO as an electrode material for

electrochemical sensing, the selection of the most appropriate synthesis procedure is of critical importance [27].

Until now, different ways and techniques have been developed to obtain RGO [26,28]. Reduction of GO to produce RGO with a smaller amount of functional groups containing oxygen compared to GO and with features more similar to those of the pristine graphene [22,23,26] can be performed either by wet chemical methods [29] or thermal treatment in inert or reductive atmosphere [30]. However, the chemically reduced GO (CRGO) usually requires toxic and strongly reducing agents, *e.g.*, hydrazine, sodium borohydride, which causes a strong agglomeration of the hydrophobic graphene flakes [31] with a significant number of impurities and structural disorders, which may have a strong impact on the quality and properties of RGO, including conductivity and electrochemical activity [28,30]. The thermal reduction of functional groups on the GO sheets is more advantageous compared to chemical reduction [32]. Besides being fast, it does not require the use of liquids as the reduction takes place in a gaseous atmosphere [32]. Moreover, obtained thermally reduced graphene oxide (TRGO) has the high exfoliation degree, large surface area, a small amount of oxygen-containing groups, and high conductivity [30].

In the present paper, the RGO synthesized by thermal treatment in ambient air conditions was used as an electrode material to produce a thermally reduced graphene oxide paste electrode (TRGOPE). The prepared electrode was utilized to examine the electrochemical behavior of bixafen using cyclic voltammetry (CV) and square-wave voltammetry (SWV) as well as to elaborate the SWV procedure for its quantification in real samples.

2 Experimental

2.1 Preparation of TRGOPE

Two paste electrodes based on TRGO synthesized in the atmosphere of ambient air (TRGOPE_{Air}) and argon (TRGOPE_{Ar}) were prepared for comparative studies. Both TRGO were synthesized according to the procedures described elsewhere [33,34]. Briefly, to prepare both TRGOPEs, each RGO and paraffin oil (Sigma-

Aldrich, Germany) in the amount of 0.5 g and 4.2 mL, respectively, were thoroughly hand-mixed in a mortar with a pestle for 15 min. The prepared pastes were left for at least 28 h for a final homogenization. The portions of the prepared pastes were packed into the Teflon (polytetrafluoroethylene, PTFE) tubes (length of 6 mm and inner diameter of 3 mm), and a silver wire was used as an electrical contact. The TRGOPEs surfaces were renewed after each recorded scan; the top layer of the used paste was removed and replaced with a new portion of the paste, and the electrode surface was polished with a weighting paper to obtain a smooth surface.

2.2 Reagents

All reagents were of analytical grade and were used as received. The aqueous solutions were prepared using triply distilled water. All solutions were stored in a dark and cold place (4 °C).

Potassium hexacyanoferrate(II) trihydrate ($K_4[Fe(CN)_6] \times 3H_2O$), potassium hexacyanoferrate(III) ($K_3[Fe(CN)_6]$), and sodium chloride (KCl) were acquired from Witko (Poland). To prepare the solution of hexacyanoferrate(III)/hexacyanoferrate(II) ($[Fe(CN)_6]^{3-/4-}$) redox marker (5.0 mmol L⁻¹), the suitable amounts of $K_4[Fe(CN)_6] \times 3H_2O$ and $K_3[Fe(CN)_6]$ were dissolved in 100.0 mmol L⁻¹ KCl solution.

The reagents used to prepare universal Britton-Robinson buffer (BRB), *i.e.*, boric acid (H_3BO_3), acetic acid (CH_3COOH), orthophosphoric acid (H_3PO_4), and sodium hydroxide (NaOH) were purchased from Avantor (Poland); a mixture of H_3BO_3 , CH_3COOH , and H_3PO_4 (all 40.0 mmol L⁻¹) has been adjusted to a pH value in the range of 2.0–12.0 with 20.0 mmol L⁻¹ NaOH.

Analytical standard of bixafen (PESTANAL[®], a purity of $\geq 98.0\%$) was purchased from Merck (Germany). A fresh standard solution of bixafen (1.0 mmol L⁻¹) was prepared weekly by dissolving the suitable amount in acetone (Avantor, Poland) due to low aqueous solubility (solubility at 20 °C in water of 0.49 mg L⁻¹ and in acetone of >250 g L⁻¹ [12]). Standard solutions of fluopyram (PESTANAL[®], a purity of $\geq 98.0\%$) and prothioconazole (PESTANAL[®], a purity of 99.9%) were also prepared in acetone.

River and tap water samples were collected from the Warta River (sampling point: Bobry, Poland) and the laboratory tap, respectively. The water samples were examined without any pretreatment and stored in the refrigerator before experiments.

2.3 Apparatus

An electrochemical impedance analyzer AutolabIII/FRA2 operated by FRA software (both Eco Chemie B.V., the Netherlands) was utilized to conduct electrochemical impedance spectroscopy (EIS) measurements, whereas Autolab PGSTAT 204 operated *via* Nova software (both Metrohm B.V., the Netherlands) was

employed to conduct CV and SWV measurements. Both analyzers were combined with an electrode stand type M164 (MTM Anko Instruments, Poland). All electrochemical experiments were carried out employing a traditional three-electrode cell configuration consisting of a TRGOPE with a diameter of 3.0 mm and geometric area (A_{geom}) of 7.1 mm² as a working electrode, silver chloride electrode (Ag|AgCl|KCl (3.0 mol L⁻¹) (Mineral, Poland) as a reference electrode, and a platinum wire (99.99%, The Mint of Poland, Poland) as a counter electrode.

The pH of BRB solutions was adjusted using a pH meter Orion Star A111 (Thermo Scientific, the Netherlands) and a Polilyte Lab pH electrode (Hamilton, Switzerland).

2.4 Measurement Procedures

The electrochemical characterization of both TRGOPEs was carried out in the $[Fe(CN)_6]^{3-/4-}$ redox marker solution (5.0 mmol L⁻¹) using EIS and CV. The EIS spectra were recorded within the frequency range of 10000–0.01 Hz with an applied sinusoidal signal of 10 mV at an open circuit potential. Fitting to the Randles equivalent circuit was performed with ZView 2.9 software. The cyclic voltammograms (CVs) for both electrodes were recorded in the potential range from -0.4 V to +1.2 V over the scan rates of 5–200 mV s⁻¹. To assess the effective surface areas (A_{eff}) of both TRGOPEs, the Randles-Sevcik equation for a reversible process was employed: $I_p = (2.69 \times 10^5) \times n^{3/2} \times A_{eff} \times D^{1/2} \times \nu^{1/2} \times c_0$, where I_p is anodic peak current (A), n is the stoichiometric number of exchanged electrons (1), ν is the potential scan rate (V s⁻¹), D is the diffusion coefficient of the $[Fe(CN)_6]^{3-/4-}$ redox probe (7.6×10^{-6} cm² s⁻¹), and c_0 is the bulk concentration of $[Fe(CN)_6]^{3-/4-}$ (5.0×10^{-6} mol cm⁻³) [35].

To examine the electrochemical behavior of bixafen at the TRGOPE, the CV and SWV were employed. CVs of bixafen were recorded in the range from -0.35 to +1.2 V with different scan rates varying from 20 to 300 mV s⁻¹ by using BRB with an optimized pH value (pH of 11.0), whereas the square-wave voltammograms (SWVs) at pH 11.0 of BRB were recorded by applying positive-going scan potential in the range from 0 to +1.2 V with the following SWV parameters: an amplitude (E_{SW}) of 100, 120, and 150 mV, a frequency (f) 80 Hz, and a step potential (ΔE_s) 3 mV.

Quantitative determination of bixafen was carried out in a selected supporting electrolyte (BRB, pH 11.0) using SWV. The standard solutions of bixafen in the concentrations interval between 0.1–25.0 μ mol L⁻¹ were prepared by dilutions of the stock bixafen solution (1.0 mmol L⁻¹) with BRB, pH 11.0. The SW voltammograms were recorded over the potential range from 0 to +1.2 V, and the following optimized SWV parameters were used: E_{SW} of 60 mV, f of 110 Hz, and ΔE_s of 4 mV. The calibration graph was constructed based on the baseline corrected SWV signals from the average value of four replicates for

each bixafen concentration. The limit of detection (LOD) and the limit of quantification (LOQ) values were estimated from the calibration graph according to IUPAC recommendations [36] using the following equations: $LOD = 3.3 \times SD_a \times b^{-1}$ and $LOQ = 10 \times SD_a \times b^{-1}$, respectively, where SD_a and b stand for the standard deviation of the intercept and the slope of the calibration graph, respectively. The sensitivity of developed procedure was assessed from the slope of the calibration graph. Precision (as a percentage RSD) and accuracy (as a recovery) were calculated for the average value ($n=4$) of the lowest measurable concentration of bixafen from the calibration graph ($0.1 \mu\text{molL}^{-1}$).

The water (river and tap) samples were spiked with the stock solution of bixafen (1.0mmolL^{-1}), and the determination of bixafen in the spiked water samples diluted with BRB, pH 11.0, was performed using the standard addition method with two consecutive additions of the bixafen stock solution. The average percentage RSD and recovery values were calculated for four replicate experiments.

The effect of interferents, *i. e.*, other fungicides such as fluopyram and prothioconazole, on bixafen SWV signal was investigated. The concentration of bixafen and tested interferents in the voltammetric cell was equal to $1.0 \mu\text{molL}^{-1}$.

3 Result and Discussion

3.1 Selection of the Electrode Material

The structural and morphological characterizations of the synthesized TRGOs using transmission electron microscopy, selected area electron diffraction, atomic force microscopy, X-ray diffraction spectroscopy, and Fourier transform infrared spectroscopy, were described elsewhere [33,34].

The electrochemical characterization of the newly prepared TRGOPE_{Air} and TRGOPE_{Ar} using EIS and CV

was performed in 5.0mmolL^{-1} $[\text{Fe}(\text{CN})_6]^{3-/4-}$ redox marker solution. Figure 1A shows a typical Nyquist diagram of real impedance (Z') vs. imaginary impedance (Z'') for TRGOPE_{Air} and TRGOPE_{Ar}. The registered plots for $[\text{Fe}(\text{CN})_6]^{3-/4-}$ were fitted to a Randles equivalent circuit (shown in the inset of Figure 1A) consisted of the solution resistance (R_s), constant phase element describing double-layer capacitance (Q_{dl}), charge transfer resistance (R_{ct}), and Warburg impedance (Z_w). The R_{ct} values of 51.1Ω for TRGOPE_{Air} and 73.9Ω for TRGOPE_{Ar} were evaluated. The results revealed almost 1.5-times lower R_{ct} value on TRGOPE_{Air} indicating slightly more accelerated charge transfer rate of $[\text{Fe}(\text{CN})_6]^{3-/4-}$ redox marker on TRGOPE_{Air} than TRGOPE_{Ar}.

The CVs of 5.0mmolL^{-1} $[\text{Fe}(\text{CN})_6]^{3-/4-}$ on both electrodes recorded with a scan rate (ν) of 50mVs^{-1} are presented in Figure 1B. As it can be seen, a pair of well-defined redox peaks was obtained at both electrodes with amplified current response on the TRGOPE_{Air} compared to TRGOPE_{Ar}. Moreover, a slightly improved electrochemical reversibility of the $[\text{Fe}(\text{CN})_6]^{3-/4-}$ redox system expressed by the peak-to-peak separation (ΔE_p) was observed on the TRGOPE_{Air} (ΔE_p of 0.120V) compared to TRGOPE_{Ar} (ΔE_p of 0.126V). Subsequently, CVs of $[\text{Fe}(\text{CN})_6]^{3-/4-}$ redox marker were recorded over the ν range of $5\text{--}200 \text{mVs}^{-1}$ for both electrodes to assess the A_{eff} values (calculation procedure described in the Section 2.4). The enhanced (1.5-times higher) A_{eff} value was evaluated for TRGOPE_{Air} (A_{eff} of 25.9mm^2) than for TRGOPE_{Ar} (A_{eff} of 17.3mm^2). In addition, A_{eff} values for TRGOPE_{Air} and TRGOPE_{Ar} were almost 3.7-times and nearly 2.5-times, respectively, higher than A_{geom} of 7.1mm^2 . All of the obtained results are consistent with the experiments conducted in our previously published works [33,34].

Further, the CVs ($\nu=100 \text{mVs}^{-1}$) and SWVs of $50.0 \mu\text{molL}^{-1}$ bixafen in the BRB, pH 11.0, were recorded on both electrodes (Figure 2). As it can be seen, the peak potential (E_p) shifted towards less positive potentials on

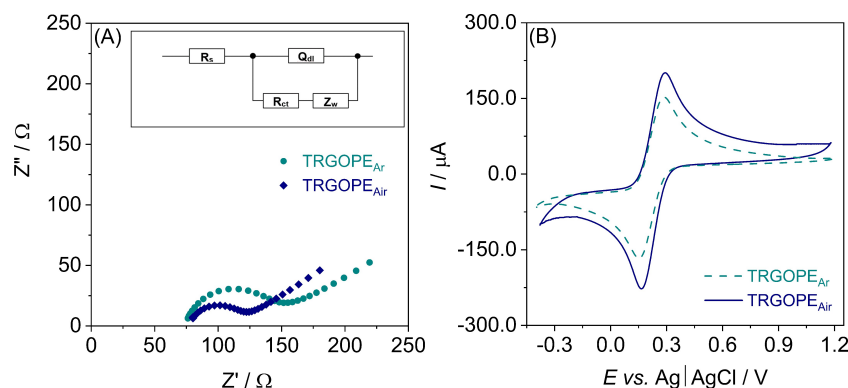


Fig. 1. (A) Nyquist plots of TRGOPE_{Ar} (●) and TRGOPE_{Air} (◆) in 5.0mmolL^{-1} $[\text{Fe}(\text{CN})_6]^{3-/4-}$ redox marker containing 100.0mmolL^{-1} KCl. Frequency range of $10000\text{--}0.1 \text{Hz}$. Inset: Randles circuit used for fitting the Nyquist plots; (B) CVs of 5.0mmolL^{-1} $[\text{Fe}(\text{CN})_6]^{3-/4-}$ in 100.0mmolL^{-1} KCl recorded on TRGOPE_{Ar} (dashed cyan line) and TRGOPE_{Air} (solid blue line) with a scan rate of 50mVs^{-1} .

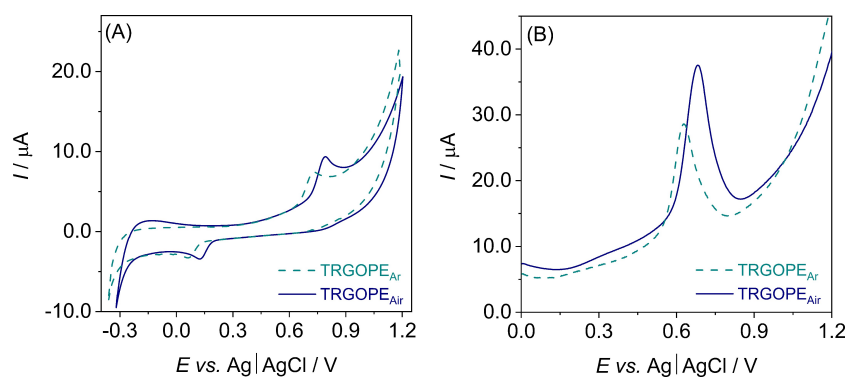


Fig. 2. (A) CVs (the first scan is depicted) and (B) SWVs of bixafen ($50.0 \mu\text{mol L}^{-1}$) in the BRB, pH 11.0, recorded on TRGOPE_{Air} (dashed cyan line) and TRGOPE_{Air} (solid blue line). CVs registered with a scan rate of 100 mV s^{-1} . SWV parameters: E_{SW} of 40 mV , f of 80 Hz , and ΔE_s of 3 mV .

TRGOPE_{Air} when compared to TRGOPE_{Air} (in CV) and ca. 1.4-times higher voltammetric responses (in SWV) were obtained on TRGOPE_{Air} than TRGOPE_{Air}.

Based on the results obtained, TRGOPE_{Air} (further denoted as TRGOPE only) was used in the subsequent measurements.

3.2 Electrochemical Behavior of Bixafen on TRGOPE

An investigation of the electrochemical behavior of bixafen ($50.0 \mu\text{mol L}^{-1}$) on the TRGOPE was conducted using CV ($\nu = 100 \text{ mV s}^{-1}$) in the BRB, pH 11.0. Voltammetric profile of bixafen vary with the number of potential cycles in CV, implying a complex electrode mechanism of an EC type, where the initial electrode reaction is followed by a chemical reaction of the electrode product. Specifically, as clearly seen in Figure 3A, a well-developed completely irreversible oxidation peak appears at a E_p of $+0.79 \text{ V}$ (peak I) in the first anodic potential sweep, which gives rise to emerging of a cathodic peak at $+0.12 \text{ V}$ (peak II') in the subsequent cathodic potential half-cycle of the cyclic voltammogram.

In the second potential cycle, a new anodic peak at $+0.17 \text{ V}$ appears (peak II), which is a counterpart of the cathodic peak II', thus representing electrode transformation of a single redox couple, formed following the initial oxidation of bixafen at $+0.79 \text{ V}$ (peak I). The voltammetric characteristics of the system II'–II resembles strongly the typical behavior of the *o*-quinone-catechol quasi-reversible redox couple [37].

Moreover, in the course of the repetitive potential cycling, a considerable decrease of the intensity of the peak I was noticed ($I_p = 3.7, 1.2, 0.73,$ and $0.49 \mu\text{A}$ for the first, second, third, and fourth potential cycle, respectively). In addition, the peak potential shifted in anodic direction ($E_p = +0.79 \text{ V}, +0.81, +0.83,$ and $+0.84 \text{ V}$, for the first, second, third, and fourth potential cycle, respectively). These data imply that the initial electrode oxidation of bixafen at $+0.79 \text{ V}$ is a complex process, followed with formation of species that partly block and inhibit the electrode surface.

Further evidences for the complexity of the electrode reaction corresponding to the peak I have been collected by studying the effect of the potential scan rate in CV,

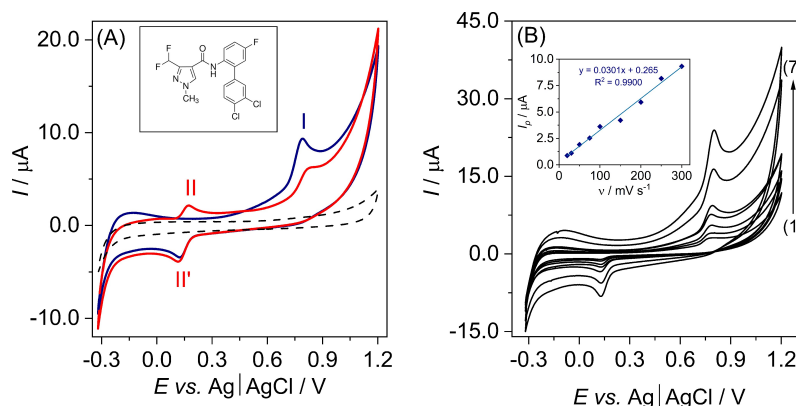


Fig. 3. (A) CVs recorded at the ν of 100 mV s^{-1} in the BRB, pH 11.0, in the absence (black dashed line) and in the presence of bixafen ($50.0 \mu\text{mol L}^{-1}$): first (blue solid line) and second (red solid line) potential scan. Inset: the chemical structure of bixafen; (B) Cyclic voltammograms of bixafen ($50.0 \mu\text{mol L}^{-1}$) recorded on the TRGOPE in the BRB, pH 11.0, at the different scan rates (ν): (1–7): $20\text{--}300 \text{ mV s}^{-1}$ (the first cycle is depicted). Inset: the linear relationship of the I_p vs. the ν .

over the interval from 20–300 mV s⁻¹ at 50.0 μmol L⁻¹ bixafen concentration in BRB, pH 11.0 (Figure 3B). It was found that the anodic E_p shifted towards more positive values (from +0.77 V to 0.80 V) with an increase of ν , while I_p increased linearly with ν ($R^2=0.9900$; inset of Figure 3B), indicating a surface-controlled process. However, the linear regression line of the logarithm of the peak current ($\log I_p$) vs. the logarithm of the scan rate ($\log \nu$) dependence exhibits a slope of 0.876 ($R^2=0.9922$). Thus, besides being followed by a chemical reaction, the electrode oxidation of bixafen is affected by adsorption of the initial reactant, and the overall process has a complex diffusion-adsorption mass transfer control.

The analysis of the electrode mechanism was further conducted under conditions of SWV, mainly by varying the SW frequency. The frequency exhibits a complex influence on both net peak current and peak potential of the process I. The net peak current increases non-linearly with the frequency (Figure 4A), due to quasi-reversible nature of the electron transfer process and the complexity arising from adsorption phenomena and the follow-up chemical reaction [38]. Plotting the dependence of the frequency-normalized net peak current ($I_p f^{-1}$) vs. the logarithm of the frequency (Figure 4B), a decreasing curve is obtained. It is a part of the descending part of the quasi-reversible maximum, the feature typical for adsorption-coupled electrode mechanisms [39]. The estimated position of the quasi-reversible maximum is within the frequencies ranging lower than 10 Hz (*i.e.*, the minimal frequency available by the instrumentation), implying a slow electrode reaction characterized with a surface formal rate constant $k_s < 10$ s⁻¹ [39]. The E_p of the net peak is also sensitive to the SW frequency, shifting in anodic direction by increasing the frequency (Figure 4C). The relationship E_p vs. $\log f$ can be associated with a regression line with a slope of 32 mV, which is in accordance with the theoretical prediction of $2.3RT/2nF$ for an electrode reaction coupled with adsorption and a follow-up chemical reaction [38].

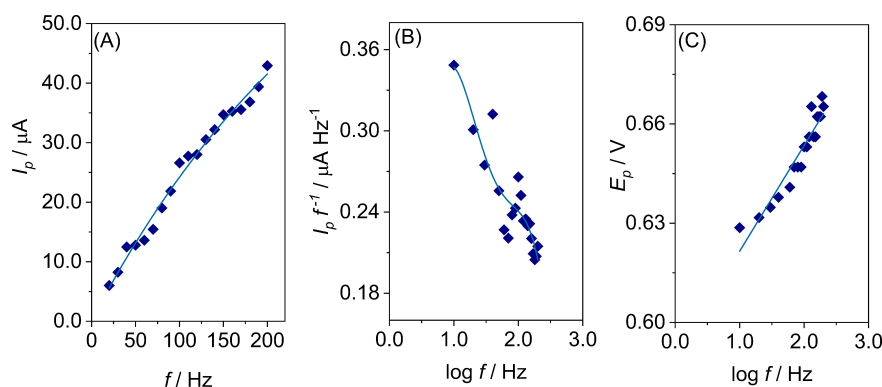


Fig. 4. The effect of the (A) SW frequency (f) on the net peak current (I_p), (B) frequency-normalized net peak current ($I_p f^{-1}$), and (C) net peak potential (E_p) of bixafen (50.0 μmol L⁻¹) in the BRB (pH 11.0). The SW amplitude is $E_{SW}=60$ mV and the step potential is $\Delta E_s=3$ mV.

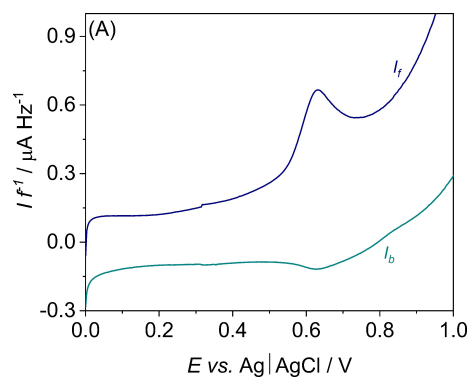


Fig. 5. The effect of the SW frequency (f) on the evolution of the frequency-normalized forward (I_f , anodic) and backward (I_b , cathodic) components of bixafen. The frequency is (A) 10, (B) 100, and (C) 200 Hz. The other conditions are as in Figure 3.

Further insights into the mechanistic aspects of the electrode mechanism can be obtained by detail inspection of the morphological evolution of the forward (I_f , anodic) and backward (I_b , cathodic) components of the SW voltammetric response for different frequencies of the potential modulation. Figure 5 displays the frequency-normalized forward ($I_f f^{-1}$) and backward ($I_b f^{-1}$) current components for the frequency of 10, 100, and 200 Hz. The normalization of the current with the frequency is done for the purpose of separating the general effect of the frequency to the thickness of the diffusion layer from the frequency effect on the kinetic parameters governing the electrode mechanism [39] which is manifested through the morphology of the voltammetric profiles. Thus, the frequency-normalized voltammetric curves shown in Figure 5 represents solely the effect of the frequency on the kinetics of the electrode mechanism. The first general feature of the frequency-normalized response is that it decreases by increasing the frequency, as a consequence of the slow electron transfer and the quasi-reversible nature of the anodic process I. More importantly the relative ratio of the peak current of the forward-to-

backward SW components (anodic-to-cathodic) increases by increasing the frequency, which is typical for an EC_{irrev} electrode mechanism, where C_{irrev} is the irreversible chemical reaction following the electrode reaction E [38]. Increasing the frequency causes the critical time of the voltammetric experiment to decrease, *i.e.*, the duration of a single potential cycle in SW voltammetry consisting of two adjacent forward (anodic) and backward (cathodic) pulses [40]. Note that SWV is very fast technique, and the critical duration of a potential cycle at frequency of 10, 100, and 200 Hz equals 100, 10, and 5 ms, respectively. Therefore, at the frequency of 10 Hz (100 ms potential cycle), there is sufficient time for significant chemical degradation of the electrochemically formed product during oxidation process I, thus, a small portion remains to be reduced back to the initial reactant by the backward (reductive) potential pulses. Consequently, the forward (oxidative) current component is significantly larger than the backward (reductive) component (Figure 5A). Shortening the time interval (*e.g.*, frequency of 100 and 200 Hz, *i.e.*, 10 and 5 ms time interval, respectively) the reductive component evolves with a complex shape (see Figure 5B and Figure 5C), as the time for chemical degradation of the electrochemical product is shorter. Though the data in Figure 5 support the assumption for the EC_{irrev} type of the electrode mechanism associated with the peak I, the complexity of the reaction pathways exceeds the EC_{irrev} scheme, due to appearance of the new, chemically reversible, and electrochemically quasi-reversible electrode process (II/II', *c.f.* Figure 3) at less positive potentials, which is the consequence of the process I.

The effect of medium pH (pH range of 2.0–12.0) adds a new clue to the overall mechanistic picture of bixafen. As it can be seen in Figure 6A, bixafen exhibited oxidation peak in the pH range of 6.0–12.0 (no oxidation peak was recorded in more acidic medium of BRB). The enhancement of the I_p of bixafen with increasing pH value (Figure 6B, \blacklozenge , left y axis) was noticed with a maximum response at pH 11.0, and thereafter, I_p decreased rapidly.

Based on the obtained results, pH 11.0 of the BRB was selected for further experiments.

Moreover, the E_p corresponding to the oxidation of bixafen shifts towards more negative potentials with increasing pH value in the range of 6.0–12.0 as it is evident from Figure 6. Thus, it can be stated that the electrode process of bixafen is pH-dependent. The plot between the E_p vs. pH (Figure 6B, \blacklozenge , right y axis) is linear ($R^2=0.9954$) according to the equation: E_p (V) = -0.0541 pH + 1.28, and the slope of -54.1 mVpH $^{-1}$ is close to the theoretical Nernstian value of 59 mVpH $^{-1}$ indicating the exchange of the equivalent number of protons and electrons participating in the electrochemical reaction [41]. In addition, the data in Figure 6 clearly show that the overall oxidation process I is energetically favored by increasing the basicity of the medium, implying that the electrode oxidation involves hydroxide ions as a reactant, or protons as a product of the electrode reaction.

The overall voltammetric behavior plausibly suggests that the initial oxidation of bixafen (peak I) is related to the dichlorobenzene moiety of the molecule, resulting in substitution of chlorine atoms with hydroxide groups, thus, forming catechol moiety, which is in agreement with known reactive oxidation pathways of other dichlorobenzene pesticides [37]. The catechol forms a chemically reversible and electrochemically quasi-reversible redox couple catechol/*o*-quinone, thus, giving rise to the new voltammetric response at the potential of about +0.12 V [37].

3.3 Optimization of SWV Parameters

To achieve a best-shaped oxidation peak of bixafen with satisfactory I_p for its determination, the optimization of the SWV parameters, *i.e.*, E_{sw} from 10 to 150 mV, f from 10 to 200 Hz, and ΔE_s from 1 mV to 10 mV, was carried out. It was noticed that the I_p increased gradually with an increase of the SW amplitude value up to 60 mV, and further, I_p was stabilized according to theory [39]. Moreover, the shift of E_p of bixafen towards more negative

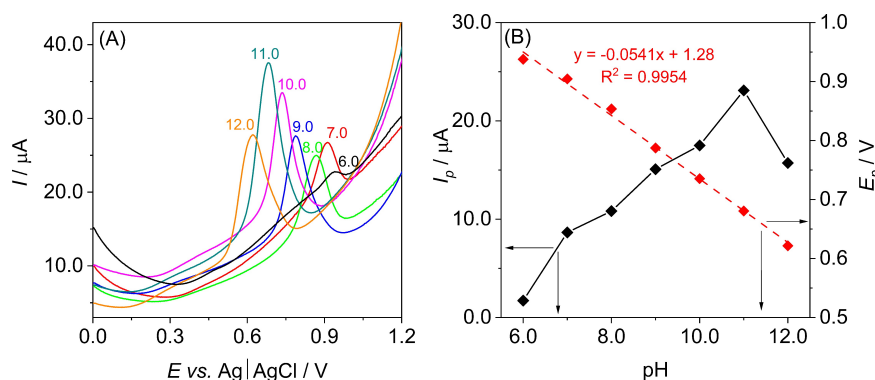


Fig. 6. (A) SWVs of bixafen ($50.0 \mu\text{molL}^{-1}$) recorded on the TRGOPE in the BRB solutions in the pH range of 6.0–12.0; (B) The corresponding dependences of I_p (\blacklozenge , left y axis) and E_p (\blacklozenge , right y axis) vs. pH. SWV parameters: E_{sw} of 40 mV, f of 80 Hz, and ΔE_s of 3 mV.

values with an increase the E_{sw} value was indicated. As the E_{sw} values greater than 60 mV did not show an increase of the height of bixafen peak, the SW amplitude of 60 mV was chosen for subsequent studies. The I_p of bixafen was found to increase in the SW frequency range of 10–200 Hz. Taking into consideration the shape and magnitude of the oxidation peak, the f of 110 Hz was selected. Moreover, the shift of the E_p towards more positive values with an increase in the f was noticed. The enhancement of the I_p of bixafen with an increase of the ΔE_s value was observed, while the peak potential was shifted towards more positive values by increasing the ΔE_s . However, when the ΔE_s value greater than 4 mV was

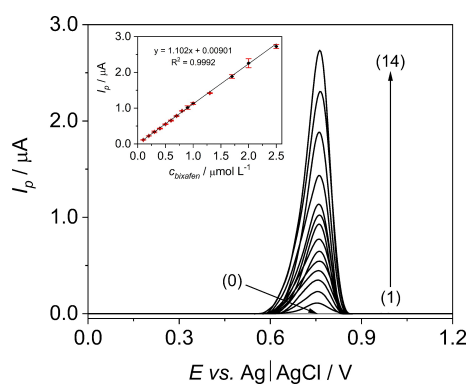


Fig. 7. Baseline corrected SWVs recorded on TRGOPE in the BRB of pH 11.0 (0) with increasing concentration of bixafen from 0.1 to 2.5 $\mu\text{mol L}^{-1}$ (1–14). SWV parameters: E_{sw} of 60 mV, f of 110 Hz, and ΔE_s of 4 mV. Inset: the corresponding calibration graph. Error bars are presented as the SD ($n=4$).

Table 2. The parameters of the calibration straight line for the bixafen determination by SWV at the TRGOPE in the BRB, pH 11.0. The measurements performed in quadruplicate ($n=4$).

Linear range	0.1–2.5 $\mu\text{mol L}^{-1}$
Coefficient of determination (R ²)	0.9992
Slope (b)	1.102 $\mu\text{A L } \mu\text{mol}^{-1}$
Intercept (a)	0.00901 μA
LOD	31.5 nmol L^{-1}
LOQ	95.3 nmol L^{-1}
Precision (RSD) ^[a]	2.9 %
Accuracy (Recovery) ^[a]	92.9 %

^[a] Precision and accuracy calculated for the concentration of bixafen of 0.1 $\mu\text{mol L}^{-1}$.

Table 3. Results obtained for the determination of bixafen in the spiked real samples by SWV at the TRGOPE using standard addition method ($n=4$).

Sample	Added	Found \pm SD/ $\mu\text{mol L}^{-1}$	RSD	Recovery
tap water	0.5 $\mu\text{mol L}^{-1}$	(0.4968 \pm 0.0040) $\mu\text{mol L}^{-1}$	0.8 %	99.4 %
	1.0 $\mu\text{mol L}^{-1}$	(1.016 \pm 0.030) $\mu\text{mol L}^{-1}$	3.0 %	101.6 %
	1.5 $\mu\text{mol L}^{-1}$	(1.505 \pm 0.035) $\mu\text{mol L}^{-1}$	2.3 %	100.3 %
river water	0.5 $\mu\text{mol L}^{-1}$	(0.4904 \pm 0.0082) $\mu\text{mol L}^{-1}$	1.7 %	98.1 %
	1.0 $\mu\text{mol L}^{-1}$	(0.9970 \pm 0.0467) $\mu\text{mol L}^{-1}$	4.7 %	99.7 %
	1.5 $\mu\text{mol L}^{-1}$	(1.508 \pm 0.076) $\mu\text{mol L}^{-1}$	5.0 %	100.5 %

applied, the distortion and broadening of the peak was observed. Well-shaped oxidation peak of bixafen was obtained at the ΔE_s of 4 mV, therefore, this value was selected as the optimal one in the further measurements.

3.4 Calibration Curve

The calibration graph was constructed based on the baseline corrected SWVs for increasing concentration of bixafen recorded in the BRB, pH 11.0, on TRGOPE (Figure 7). Based on the constructed calibration graph, the analytical parameters towards bixafen determination, such as linearity, LOD, LOQ, sensitivity, precision, and accuracy, were evaluated, and the validation parameters of the calibration straight line are shown in Table 2.

As it can be seen, bixafen on TRGOPE showed a linearity in the range of 0.1–25.0 $\mu\text{mol L}^{-1}$ ($R^2=0.9992$) with the sensitivity of 1.102 $\mu\text{A L } \mu\text{mol}^{-1}$, low LOD of 31.5 nmol L^{-1} , and LOQ of 95.3 nmol L^{-1} . Moreover, the percentage RSD and recovery estimated for the average value ($n=4$) of the lowest measurable concentration of bixafen from the calibration graph (0.1 $\mu\text{mol L}^{-1}$) were equal to 2.9 % and 95.3 %, respectively, confirming that the proposed procedure for the bixafen determination on the TRGOPE is highly precise and accurate.

3.5 Real Sample Analysis

The usefulness of the optimized and validated procedure for the SWV determination of bixafen on TRGOPE was verified by the analysis of bixafen in the spiked real (tap and river water) samples. As bixafen was not detected in the tested samples, spiking experiments were performed, and bixafen concentrations were analyzed using standard addition method. As evident from Table 3, the found (calculated) concentrations of bixafen in both tested samples were very close to the added (spiked) values. In addition, low RSD values (the RSD did not exceed 5.0 %) confirmed highly repetitive measurements with the use of the TRGOPE. Moreover, acceptable recovery values were achieved for bixafen in examined real samples indicating no significant matrix effect from the tested samples on bixafen performance. Accordingly, the applicability of the procedure for the bixafen determination in the tested samples using TRGOPE was evidenced.

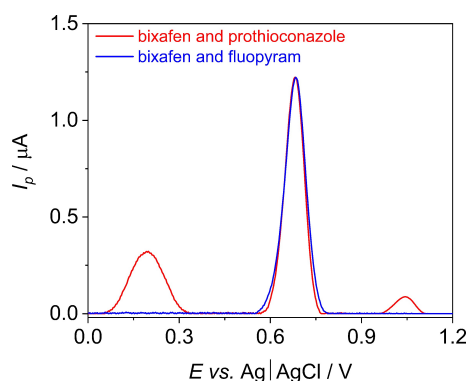


Fig. 8. SWVs of bixafen ($1.0 \mu\text{mol L}^{-1}$) recorded on the TRGOPE in the presence of fluopyram (solid blue line) and prothioconazole (solid red line). The concentration of both interferents was equal to concentration of bixafen. SWV parameters: E_{SW} of 60 mV, f of 110 Hz, and ΔE_s of 4 mV.

3.6 Interference Study

Lastly, the selectivity of the developed procedure towards bixafen determination was tested. For that purpose, SWV measurements were performed in the presence of other fungicides (fluopyram and prothioconazole) that are present together with bixafen in the commercial formulation Ascra[®] Xpro 260 EC. It was found that, in the tested potential window, prothioconazole ($1.0 \mu\text{mol L}^{-1}$) gave two oxidation peaks at the E_p of +0.19 and +1.0 V, whereas fluopyram ($1.0 \mu\text{mol L}^{-1}$) did not show the electrochemical activity. Thus, as can be seen in Figure 8, it was possible to assess bixafen in the presence of tested interferents. Accordingly, the proposed procedure is characterized by a good selectivity towards bixafen determination.

4 Conclusions

The electroanalytical study of the fungicide bixafen using paste electrode based on the reduced graphene oxide synthesized by thermal treatment in ambient air conditions is presented for the first time. To characterize the mechanism of the underlying electrode process of bixafen, cyclic voltammetry and square-wave voltammetry were employed. The studies manifested that besides being followed by a chemical reaction, the electrode oxidation of bixafen is affected by adsorption of the initial reactant, and the overall process has a complex diffusion-adsorption mass transfer control. The voltammetric behavior plausibly suggests that the initial oxidation of bixafen is related to the dichlorobenzene moiety of the molecule, resulting in substitution of chlorine atoms with hydroxide groups, thus, forming catechol moiety that forms a chemically reversible and electrochemically quasi-reversible redox couple catechol/*o*-quinone. Further, SWV was employed to develop a procedure for bixafen sensing. The optimized SWV procedure enables determination of bixafen with the linear range of $0.1\text{--}2.5 \mu\text{mol L}^{-1}$ in the

alkaline medium (the BRB, pH 11.0) together with a very low LOD of 31.5 nmol L^{-1} and a sensitivity of $1.102 \mu\text{A L } \mu\text{mol}^{-1}$. The developed simple and rapid methodology was effectively utilized for the bixafen determination in the spiked water (river and tap) samples and in the presence of other fungicides that are components of the commercial formulation together with bixafen. The TRGOPE in combination with the SWV technique acts as a good substitute for chromatographic techniques that are laborious and more costly than electroanalytical techniques.

Acknowledgements

MB would like to acknowledge the financial support of the National Science Centre (NCN), Cracow, Poland (Grant no. UMO-2014/15/N/ST4/02285).

Data Availability Statement

The data that support the findings of this study are available from the corresponding author upon reasonable request.

References

- [1] M. Yamashita, B. Fraaije, *Pest Manag. Sci.* **2018**, *74*, 672–681.
- [2] S. M. Yahaya, A. Y. Mardiyaya, *Biomed. J. Sci. Tech. Res.* **2019**, *13*, 10192–10200.
- [3] A. Brenet, R. Hassan-Abdi, N. Soussi-Yanicostas, *Chemosphere* **2021**, *265*, 128781.
- [4] C. A. Berdugo, U. Steiner, H. W. Dehne, E. C. Oerke, *Pestic. Biochem. Physiol.* **2012**, *104*, 171–177.
- [5] A. Abad-Fuentes, E. Ceballos-Alcantarilla, J. V. Mercader, C. Agulló, A. Abad-Somovilla, F. A. Esteve-Turrillas, *Anal. Bioanal. Chem.* **2015**, *407*, 4207–4211.
- [6] W. Li, M. Yuan, Y. Wu, X. Liu, *Environ. Res.* **2020**, *189*, 109923.
- [7] A. Lalève, S. Gamet, A. S. Walker, D. Debieu, V. Toquin, S. Fillingier, *Environ. Microbiol.* **2014**, *16*, 2253–2266.
- [8] Y. Shen, Z. Li, Q. Ma, C. Wang, X. Chen, Q. Miao, C. Han, *J. Agric. Food Chem.* **2016**, *64*, 3901–3907.
- [9] F. Dong, X. Chen, X. Liu, J. Xu, Y. Li, W. Shan, Y. Zheng, *J. Chromatogr. A.* **2012**, *1262*, 98–106.
- [10] M. Yuan, W. Li, P. Xiao, *Environ. Sci. Pollut. Res.* **2021**, *28*, 36303–36313.
- [11] M. Anastassiadou, G. Bernasconi, A. Brancato, L. Carrasco Cabrera, L. Greco, S. Jarrah, A. Kazocina, R. Leuschner, J. O. Magrans, I. Miron, S. Nave, R. Pedersen, H. Reich, A. Rojas, A. Sacchi, M. Santos, A. Stanek, A. Theobald, B. Vagenende, A. Verani, *EFSA J.* **2020**, *18*, 5998.
- [12] European Food Safety Authority, Conclusion on the peer review of the pesticide risk assessment of the active substance bixafen, *EFSA J.* **2012**, *10*, 2917.
- [13] A. Gulkowska, I. J. Buerge, T. Poiger, *Anal. Bioanal. Chem.* **2014**, *406*, 6419–6427.
- [14] Y. L. Wu, R. X. Chen, Y. Zhu, J. Zhao, T. Yang, *J. Chromatogr. B* **2015**, *989*, 11–20.
- [15] R. Özcan, Ç. Büyükpınar, S. Bakırdere, *J. Environ. Sci. Heal. - Part B Pestic. Food Contam. Agric. Wastes.* **2020**, *55*, 1041–1047.

- [16] E. Hakme, A. Lozano, S. Uclés, M. M. Gómez-Ramos, A. R. Fernández-Alba, *J. Chromatogr. A* **2018**, *1573*, 28–41.
- [17] S. Nussbaumer, P. Bonnabry, J. L. Veuthey, S. Fleury-Souverein, *Talanta* **2011**, *85*, 2265–2289.
- [18] F. Scholz, *ChemTexts* **2015**, *1*, 1–24.
- [19] S. Michalkiewicz, A. Skorupa, M. Jakubczyk, *Materials* **2021**, *14*, 7630.
- [20] J. Gaidukevic, R. Aukstakojyte, J. Barkauskas, G. Niaura, T. Murauskas, R. Pauliukaite, *Appl. Surf. Sci.* **2022**, *592*, 153257.
- [21] A. K. Geim, K. S. Novoselov, *Nat. Mater.* **2007**, *6*, 183–191.
- [22] S. Farah, A. Farkas, J. Madarász, K. László, *J. Therm. Anal. Calorim.* **2020**, *142*, 331–337.
- [23] S. M. S. Al-Mufti, A. Almontasser, S. J. A. Rizvi, *Mater. Today Proc.* **2022**, *57*, 1713–1718.
- [24] A. M. A. D. Assis, K. S. da Silva, M. K. S. Araújo, D. C. S. Sales, M. C. Ferreira, A. C. V. de Araújo, W. M. de Azevedo, E. H. L. Falcão, *Colloids Surfaces A* **2020**, *599*, 124837.
- [25] M. Rezaee, L. C. Tsai, A. Elyasigorji, M. I. Haider, A. Yazdi, N. P. Salowitz, *Eng. Fract. Mech.* **2021**, *243*, 107525.
- [26] N. Sharma, S. Monga, M. Shkir, Y. K. Mishra, R. S. Katiyar, A. Singh, *Mater. Sci. Semicond. Process.* **2022**, *142*, 106478.
- [27] D. Minta, Z. González, S. Melendi-Espina, G. Gryglewicz, *Surf. Interfaces* **2022**, *28*, 101606.
- [28] S. Ram Joshi, J. Lee, G. H. Kim, *Mater. Lett.* **2021**, *292*, 129649.
- [29] C. K. Chua, M. Pumera, *Chem. Soc. Rev.* **2014**, *43*, 291–312.
- [30] O. Jankovský, M. Lojka, M. Nováček, J. Luxa, D. Sedmidubský, M. Pumera, J. Kosina, Z. Sofer, *Green Chem.* **2016**, *18*, 6618–6629.
- [31] A. Shalaby, D. Nihtianova, P. Markov, A. D. Staneva, R. S. Jordanova, Y. B. Dimitriev, *Bulg. Chem. Commun.* **2015**, *47*, 291–295.
- [32] A. Kalfa, T. R. Penki, I. Cohen, N. Shpigel, E. Avraham, D. Aurbach, D. Liang, Q. Wu, H. Wang, Y. Xiang, *Desalination* **2020**, *492*, 114599.
- [33] M. Brycht, A. Leniart, J. Zavašnik, A. Nosal-Wiercińska, K. Wasiński, P. Pórolniczak, S. Skrzypek, K. Kalcher, *Electrochim. Acta* **2018**, *282*, 233–241.
- [34] M. Brycht, A. Leniart, J. Zavašnik, A. Nosal-Wiercińska, K. Wasiński, P. Pórolniczak, S. Skrzypek, K. Kalcher, *Anal. Chim. Acta* **2018**, *1035*, 22–31.
- [35] A. J. Bard, L. R. Faulkner, in *Electrochemical Methods: Fundamentals and Applications*, 2nd ed. (Ed.: D. Harris), Wiley-VCH, New York, **2000**.
- [36] J. Mocak, A. M. Bond, S. Mitchell, G. Scollary, A. M. Bond, *Pure Appl. Chem.* **1997**, *69*, 297–328.
- [37] N. Rabaoui, S. Kacem, M. El Khames Saad, E. Elaloui, Y. Moussaoui, *Mod. Chem. Appl.* **2017**, *5*, 1000234.
- [38] V. Mirčeski, M. Lovrić, *Croat. Chem. Acta* **2000**, *73*, 305–329.
- [39] V. Mirceski, S. Komorsky-Lovric, M. Lovric, in *Square-Wave Voltammetry: Theory and Applications*, 1st ed. (Ed.: F. Scholz), Springer-Verlag, Berlin Heidelberg, **2007**.
- [40] V. Mirceski, S. Skrzypek, L. Stojanov, *ChemTexts* **2018**, *4*, 1–14.
- [41] P. Zuman, in *The Elucidation of Organic Electrode Processes*, 1st ed. (Ed.: L. Meites), Academic Press, New York, London, **1969**.

Received: August 31, 2022

Accepted: October 13, 2022

Published online on November 11, 2022